The Astrophysical Journal, 757:167 (10pp), 2012 October 1 doi:10.1088/0004-637X/757/2/167

THREE-DIMENSIONAL STRUCTURE AND EVOLUTION OF EXTREME-ULTRAVIOLET BRIGHT POINTS OBSERVED BY *STEREO*/SECCHI/EUVI

Ryun-Young Kwon[1,2], Jongchul Chae[3], Joseph M. Davila[2], Jie Zhang[4], Yong-Jae Moon[5], Watanachak Poomvises[1,2], and Shaela I. Jones[2,6]

[1] Department of Physics, Institute for Astrophysics & Computational Sciences, Catholic University of America, 620 Michigan Avenue, Washington, DC 20064, USA
[2] NASA Goddard Space Flight Center, Solar Physics Laboratory, Code 671, Greenbelt, MD 20771, USA; ryunyoung.kwon@nasa.gov
[3] Astronomy Program, Department of Physics and Astronomy, Seoul National University, Seoul, Republic of Korea
[4] School of Physics, Astronomy and Computational Sciences, George Mason University, Fairfax, VA 22030, USA
[5] School of Space Research, Kyung Hee University, Yongin 446-701, Republic of Korea
[6] Department of Physics, University of Maryland, College Park, MD 20740, USA
Received 2012 March 30; accepted 2012 August 2; published 2012 September 14

ABSTRACT

We unveil the three-dimensional structure of quiet-Sun EUV bright points and their temporal evolution by applying a triangulation method to time series of images taken by SECCHI/EUVI on board the *STEREO* twin spacecraft. For this study we examine the heights and lengths as the components of the three-dimensional structure of EUV bright points and their temporal evolutions. Among them we present three bright points which show three distinct changes in the height and length: decreasing, increasing, and steady. We show that the three distinct changes are consistent with the motions (converging, diverging, and shearing, respectively) of their photospheric magnetic flux concentrations. Both growth and shrinkage of the magnetic fluxes occur during their lifetimes and they are dominant in the initial and later phases, respectively. They are all multi-temperature loop systems which have hot loops ($\sim 10^{6.2}$ K) overlying cooler ones ($\sim 10^{6.0}$ K) with cool legs ($\sim 10^{4.9}$ K) during their whole evolutionary histories. Our results imply that the multi-thermal loop system is a general character of EUV bright points. We conclude that EUV bright points are flaring loops formed by magnetic reconnection and their geometry may represent the reconnected magnetic field lines rather than the separator field lines.

Key words: Sun: corona – Sun: transition region – Sun: UV radiation

Online-only material: color figures

1. INTRODUCTION

It has been suggested that frequent magnetic reconnections owing to small-scale opposite magnetic flux concentrations should be a potential source to maintain the high temperature (>1 MK) of the solar corona (Schrijver et al. 1998; von Rekwski et al. 2006, and reference therein). EUV bright points (hereafter BPs) are the consequence of the small-scale magnetic reconnections and observed as an ubiquitous feature in active Sun, quiet Sun, and coronal hole regions, with a typical temperature below 2 MK (Golub et al. 1974, 1975, 1976; Zhang et al. 2001). BPs have been typically observed above two opposite longitudinal magnetic flux concentrations (Krieger et al. 1971) of which the total unsigned magnetic fluxes show increase or decrease patterns (e.g., Webb et al. 1993, and references therein). BPs have been observed in ephemeral active regions consisting of several small emerging magnetic bipoles having a flux of about 10^{18}–10^{20} Mx (Harvey & Martin 1973; Golub et al. 1974, 1977; Martin & Harvey 1979; Schrijver et al. 1998). On the other hand, Webb et al. (1993) reported that most of BPs are associated with two opposite magnetic flux concentrations converging and canceling, which is thought to be a cause of magnetic reconnection and subsequent submergence of magnetic fluxes (Chae et al. 2002, 2004). Recently, Madjarska et al. (2003) showed that a BP first appeared when two opposite magnetic flux concentrations were about 7000 km apart and disappeared around the time when one flux concentration disappeared. In addition, they found that there is a remarkable correlation between the intensity of a BP and the unsigned total magnetic flux during its life.

Based on the observational facts described above, several theoretical models have explained the formation and evolution of BPs. Priest et al. (1994) proposed a model, the so-called converging flux model, in order to explain observational reports of the converging and canceling magnetic flux concentrations. In contrast, the separator reconnection model propounded by Longcope (1998) suggests shearing motions of photospheric magnetic flux concentrations with background magnetic fields as a necessary condition for the occurrence of magnetic reconnection. These two models seem to be strongly constrained by the three-dimensional (3D) structure of BPs. For instance, the converging flux model predicts that the geometry of a BP strongly depends on the distance of an underlying magnetic bipole and its height should decrease over time, owing to converging motions of magnetic flux concentrations (Kwon et al. 2010). On the other hand, the separator reconnection model allows the size of a BP to exceed the distance of two magnetic flux concentrations so that the geometry of a BP does not have to decrease (Longcope et al. 2001), even if the two magnetic flux concentrations converge.

Recently, the first stereoscopic analysis of BPs was done by Kwon et al. (2010) using simultaneous observation performed by *STEREO*/SECCHI/EUVI and they showed multi-layered thermal structure of BPs, whose outer loops are hotter than inner ones (see also, Simon & Noyes 1972; Simon et al. 1974; Habbal & Withbroe 1981; van Driel-Gesztelyi et al. 1996). According to their results, the BPs seen in the 171, 195, and 284 Å images are loop shaped and their average heights above the photosphere are 5.1, 6.7, and 6.1 Mm, respectively. The heights of the loops are approximately half of the projected lengths on the image

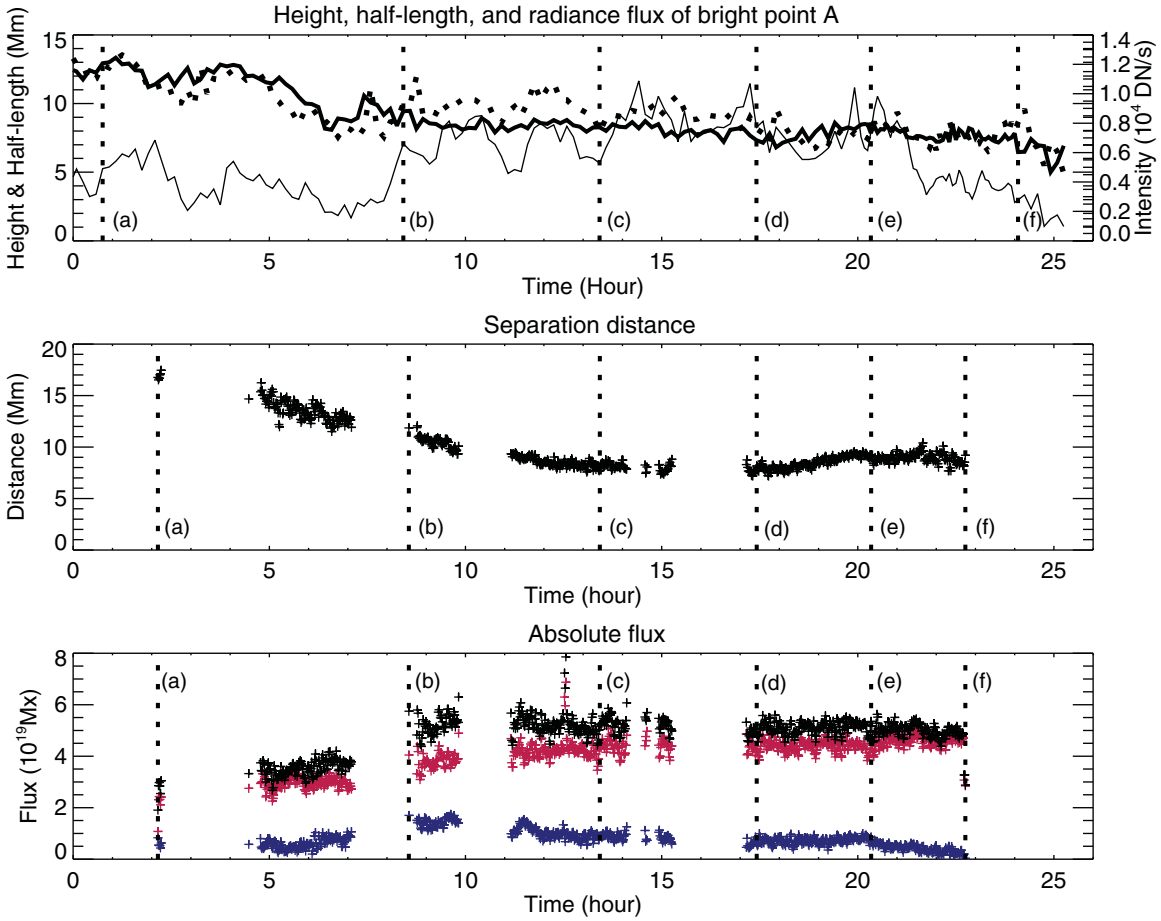

Figure 1. Temporal evolution of the physical parameters of the case A BP. The *x*-axis refers to the relative time from when the BP first appeared. The top panel shows the height (solid), half-length (dotted), and integrated intensity (thin solid) variations. The middle panel represents the distance between two opposite magnetic flux concentrations in units of Mm and the bottom panel shows the unsigned magnetic flux variation in units of 1×10^{19} Mx. The black, blue, and red colors refer to the unsigned total, negative, and positive magnetic fluxes, respectively. The letters from (a) to (f) refer to the specific times which show some noticeable morphological changes (see the text) in Figure 2.

(A color version of this figure is available in the online journal.)

planes. The heights of BPs in the 304 Å images are the lowest among the four passbands with an average of 4.4 Mm and seem to be commonly associated with the legs of the loop-shape BPs. These characteristics are similar to the semi-circular loops and temperature stratification found in the flaring loop reported by Masuda et al. (1994). Because of these consistency, it may be concluded that BPs are flaring loop systems formed by magnetic reconnection and they may not be different from the normal flares (Shimojo & Shibata 1999, and reference therein).

The main purpose of the present work is to reveal the evolution of 3D structure of EUV BPs, seeking the changes in the height and length. The physical properties of the underlying magnetic flux concentrations are inspected to see what determines their 3D structures. From the analysis, we present three distinct changes in the height: decreasing, increasing, and steady. In addition, we are aiming to generalize the characteristics of the 3D structure of EUV BPs, such as multi-thermal and semi-circular loop system found by an analysis of snapshot images (Kwon et al. 2010) to the evolutionary history in whole lives. The next section describes the data and methods to determine the 3D structure and to measure properties of their underlying magnetic flux concentrations. Section 3 shows the three distinct changes in the 3D structures and Section 4 is devoted to detailed discussions on our findings. Finally, a brief conclusion is given in Section 5.

2. DATA AND ANALYSIS

The heights, lengths, and intensities of EUV BPs are measured using images taken by the Extreme UltraViolet Imager (EUVI; Wülser et al. 2004) on board the *Solar TErrestrial RElations Observatory* (*STEREO*) spacecraft (Howard et al. 2008). *STEREO* consists of twin spacecraft moving ahead (hereafter *SC*/*A*) and behind (*SC*/*B*) the Earth around the Sun. EUVI instruments provide two simultaneous solar images at different view points with four passbands at 171, 195, 284, and 304 Å. We used the time series of images taken from 2008 March 21 to 23, when the separation angle of the two spacecraft was about 47°. Since the *SC*/*A* and *B* are located at different distances from the Sun, they have different spatial resolutions. The pixel size of EUVI instruments is 1.″6 and the distances of the *SC*/*A* and *B* from the Sun were 1.44×10^8 and 1.51×10^8 km at that time, so that one pixel of *SC*/*A* and *B* corresponds to about 1.11 and 1.16 Mm, respectively. The time cadences of the images at 171, 195, 284, and 304 Å were typically 2.5, 10, 20, and 2.5 or 10 minutes, respectively. In addition, we used full-disk 1 minute magnetograms taken by *SOHO*/MDI in order to examine properties of photospheric magnetic fluxes associated with analyzed BPs.

We employed a method developed by Kwon et al. (2010) to measure heights of BPs. To measure a height and its variation for

a BP, a sequence of sub-images centered on a BP is extracted with a size of 32 × 32 pixels and the background emission and noise are removed. After that the true signal of the BP is obtained and the center of the BP is determined by the center of gravity method. The two lines of sight from two spacecraft to the centers of the BP are determined and the height is measured by determining the skew of the two lines of sight. After subtracting the background and the noise from the original images, the length and integrated intensity of the BP are measured. The length of a BP is defined as the maximum length between two points comprising the boundary of a BP on *SC*/*A* and *B* images, since the projection effect may reduce the length on the image planes. The intensity is defined as the sum of intensities over the pixels inside the boundary of a BP on *SC*/*A* images. A detailed explanation of the method is given in Kwon et al. (2010).

Now, we would like to explain a method to determine photospheric magnetic fluxes and distances between two opposite magnetic flux concentrations associated with BPs. In order to minimize the geometrical distortion of longitudinal magnetic fields due to the spherical shape of the Sun, we only selected BPs whose heliocentric angles are equal to or less than 30°. We took averages over three frames of magnetograms taken within 3 minutes to remove high-frequency features on the magnetograms. Moreover, pixels with the unsigned values below 15 G are set to zero. The center of each magnetic element is determined by the center of gravity method and the distance represents the length between the two centers projected on the image planes. Finally, the magnetic flux of each pole is determined by integrating the flux density over the region masked.

Meanwhile, we need to correct the recorded time on each spacecraft. Since the distances between the Sun and the spacecraft are generally different, the light traveling times are different, and the times recorded in the fit headers may be different for a specific event. In order to remove this discrepancy, the times are compensated for by the differences of light traveling time from the Sun so that each time corresponds to what would be observed at Earth's position.

3. RESULTS

Heights of 13 EUV BPs were measured during their entire lives. The lifetimes range from 9 to 47 hr with an average of 20 hr and the heights are in the range of 4–18 Mm with an average of 8 Mm. Our analysis reveals that there exist all possible height changes, rather than a typical pattern, and these are increasing, decreasing, and steady. BPs were categorized into three types according to the height changes in their initial phases and it is interesting to note that there were no dominant patterns: 5, 4, and 4 events for the three types, respectively. In order to carry out a detailed study of the evolution of BPs, we selected three BPs from each type, whose heliocentric angles on the MDI magnetograms are equal to or less than 30°. In the following three sections, we show the case studies of three BPs at the 195 Å passband. Cases A, B, and C refer to the three types, decreasing, increasing, and steady in height in their initial phases, respectively.

3.1. Case A

The first case shows the significant decreasing pattern in height in its initial phase within about 13 hr. This BP lasts for about 25 hr. Figure 1 shows the height (thick-solid), half-length (dotted), and intensity (thin-solid) of this BP in the top panel, the separation distance of the underlying magnetic flux concentrations with plus symbols in the middle panel, and the absolute values of negative (blue), positive (red), and total (black) magnetic fluxes in the bottom panel. Image cubes in Figure 2 show the morphologies of this BP and the magnetic flux concentrations observed by *SC*/*B*, *A*, and *SOHO*/MDI, from left to right, at the times (a–f) denoted in Figure 1. These figures reveal that this BP is a faint and large loop system in the initial phase, for instance at (a), and evolves into a brighter and smaller one (b–e). The height and half-length are initially about 13 Mm at (a) and continuously decrease to about 8 Mm at (c). In the remaining lifetime, the height and half-length are still continuously decreasing from 8 to 6 Mm, but it is not so

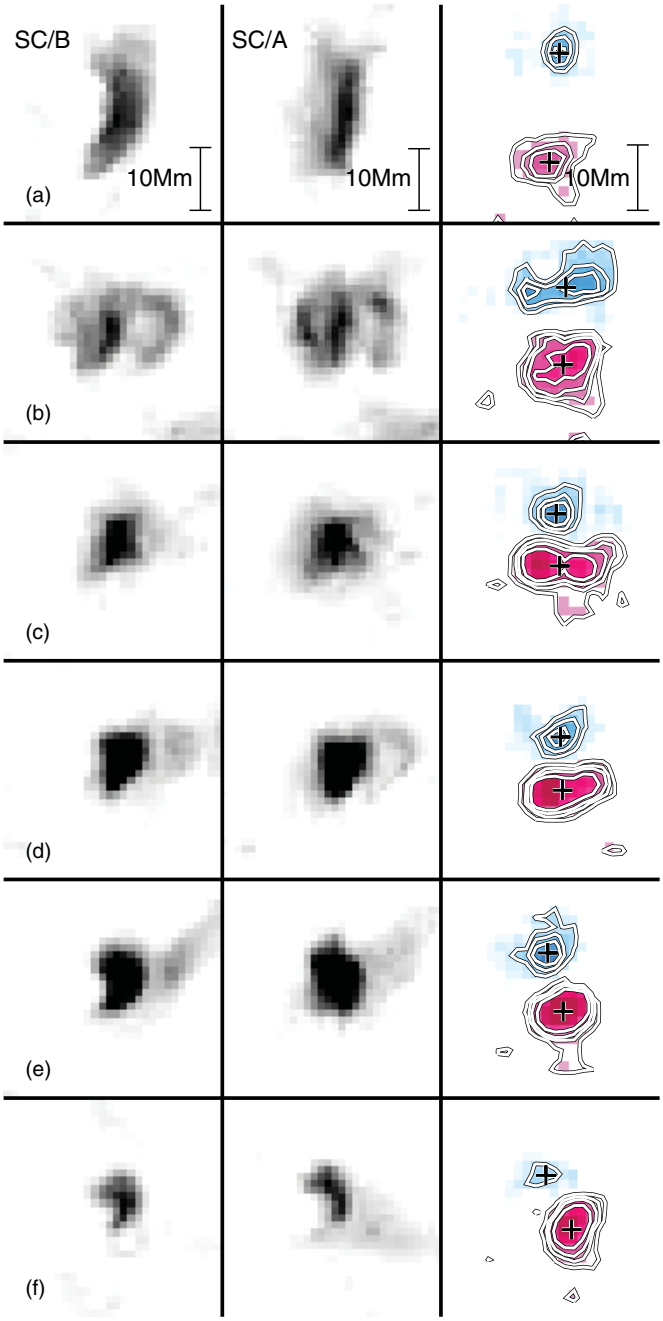

Figure 2. Morphological variation of the case A BP at the times (a) to (f) in Figure 1. The first and the second column show the BP observed by *SC*/*A* and *SC*/*B*, respectively. The third column shows a time series of photospheric longitudinal magnetograms observed by *SOHO*/MDI. Red and blue colors refer to the positive and negative fluxes, respectively.

(A color version of this figure is available in the online journal.)

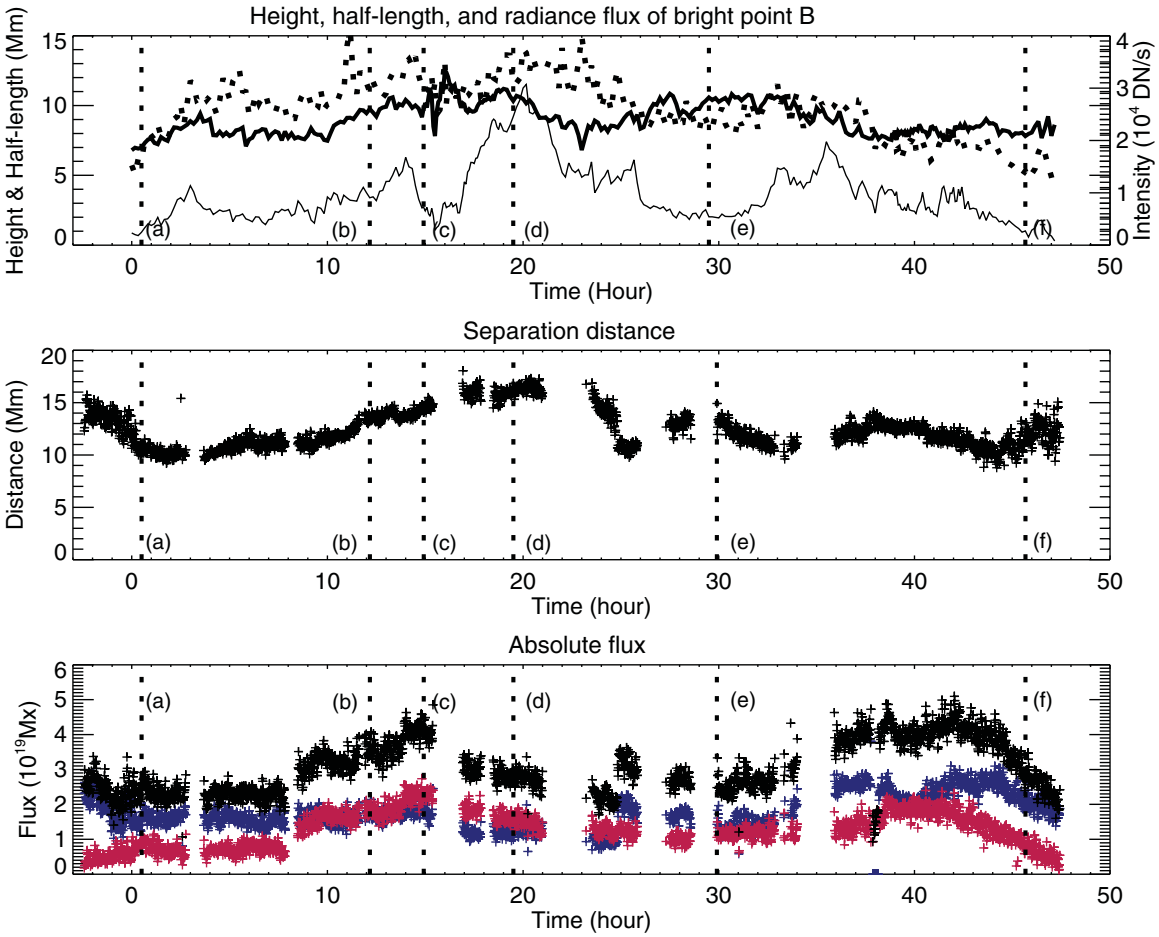

Figure 3. Temporal evolution of the physical parameters of case B. Other explanations are the same as Figure 1.
(A color version of this figure is available in the online journal.)

significant. The intensity significantly increases from (b). It has several peaks and finally decreases from around (e). The two opposite underlying magnetic flux concentrations are placed 17 Mm apart initially at (a) and converge toward each other continuously to a distance of about 8 Mm at (c). The change in the separation distance seems to be consistent with the changes in the height and length. The magnetic flux concentrations are initially small and weak, and the positive flux is larger than the negative one at (a). After that, both the fluxes grow continuously from (a) to (b) and a new positive flux emerges at the left-hand side of the field of view at (b) in Figure 2. As a result, the loop system becomes complicated, being made up of several loops, at least three. The negative flux decreases significantly from time (d) and finally it almost disappears.

In the later phase after time (c), the changes in the height, length, and separation distance seem to be steady. In this phase, the magnetic flux concentrations show weak shearing motions: the negative flux moves to the left-hand side of the positive one and the axis of the loop system is rotated at the same time (Figure 2).

3.2. Case B

The lifetime of case B is 47 hr which is about twice that of case A. Figures 3 and 4 show that this BP comes into sight first as a small and faint loop system and turns out to be a larger and brighter loop system, which is different from case A. In the initial phase within about 13 hr, the height (half-length) increases from 7 Mm (6 Mm) at (a) to 10 Mm (11 Mm) at (c). The intensity of this BP has several peaks and the maximum peak is at time (d) when the size of the BP is maximum. The separation distance of the underlying magnetic flux concentrations increases from (a) to (c), similar to the size of the BP which increases in the same phase. The magnetic flux concentrations are initially small and weak and the positive flux significantly increases from (a) to (c) while the negative flux does not change much. The positive flux decreases at (c). From (b) to (d) in Figure 4, a new negative flux appears at the upper right side of the field of view and a new loop system rises up between an old positive flux and the new negative flux. The newly connected loop system is seen until time (d), then it disappears with its underlying negative flux. On the other hand, the later phase of the evolution from (d) to (f) shows that the separation distance and the size of the BP decrease together.

3.3. Case C

Case C is clearly distinguished from cases A and B. As seen from Figure 5, its height changes little during its lifetime of 13 hr, the shortest among the three cases. The minimum height is about 8 Mm and the maximum height is about 10 Mm, so the variation in height does not exceed 2 Mm. The change in half-length is small in which the minimum and maximum lengths are about 8 and 12 Mm, respectively. The intensity variation is similar to those of the other cases; the BP first appears as a faint loop system, reaches its maximum intensity at (d), and then

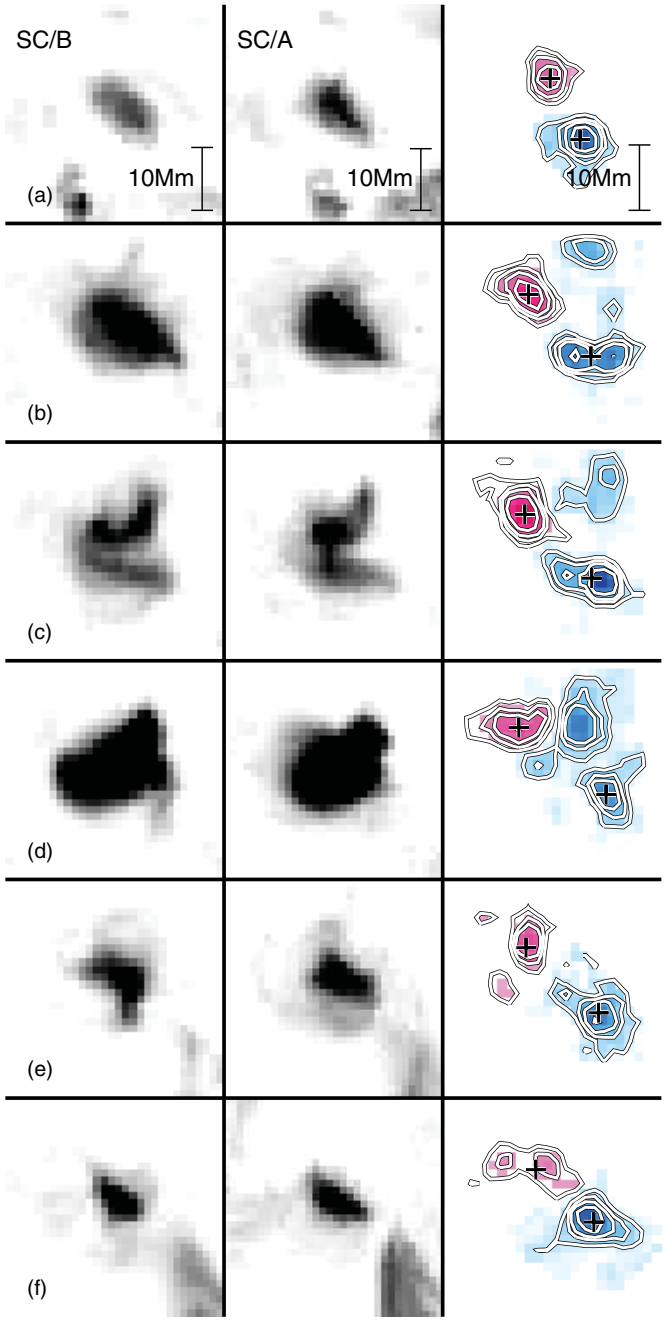

Figure 4. Morphological variation of case B at the times (a)–(f) in Figure 3. Other explanations are the same as Figure 2.

(A color version of this figure is available in the online journal.)

fades during the rest of its life. A small change in the separation distance of the two opposite magnetic flux concentrations is found in consistency with the height and length. In the initial phase, the separation distance in Figure 5 remains almost the same, but it begins to decrease a little at (c). After $t = 9$ hr, it seems to increase slightly. Figure 6 suggests that this BP should be associated with a shearing motion of the magnetic flux concentrations. Initially, the negative and positive fluxes are aligned in the north–south direction and then the negative flux moves to the right side of the positive flux. This motion is consistent with the orientation of the BP observed by SC/A and SC/B. The axis of the loop system is initially aligned in the direction around 1 o'clock and then, with the movements of the magnetic flux concentrations, the axis rotates counterclockwise. Its final orientation is around 10 o'clock. The variations of the magnetic fluxes and the 3D structure are simpler than those of the other cases. Like the other cases, the flux increases in the initial phase and then decreases in its later half phase.

4. DISCUSSION

In the previous section, we have presented temporal evolutions of the heights of three EUV BPs. Kwon et al. (2010) presented two ways to estimate errors in heights. The first one is an analytical way to derive an intrinsic error in carrying out a triangulation. This error depends on the separation angle (Θ) between the two spacecraft, the measurement error (Δ_2) in measuring the center of a BP on an SC/B image, and the heliocentric angle (α_1) of a BP observed by SC/A. The distance error in the line of sight of SC/A is given by $\Delta X_1 = \Delta_2/\sin\Theta$ and the height error Δh is approximately $\Delta X_1 \cos\alpha_1$. The separation angle of the two spacecraft during the observing period was about 47° and the measurement error Δ_2 was about 0.6 Mm (0.5 pixel on SC/B image), giving the intrinsic height error of about 0.82 Mm. Another one is an empirical way to estimate the measurement error in height using independent measurements at 195 and 284 Å passbands. Because the filter response functions of 195 and 284 Å passbands have similar peak temperatures ($10^{6.2}$ and $10^{6.4}$ K, respectively), the two passband images may represent similar plasma structures and the two heights may be well correlated with each other. The differences between the heights may be due to intrinsic differences plus random errors, so that the differences of the two heights may tell us the maximum random error. The bottom-right panel in Figure 9 compares the heights between BPs at 195 and 284 Å passbands and shows their linear regression (dotted line) and height deviations (solid lines). In this way, the measurement errors are found to be about 0.81 and 0.65 Mm at 195 and 284 Å passbands, respectively. From the intrinsic and empirical errors, we conclude that the error in height may not exceed 1 Mm.

One of the most prominent findings is that there are three distinct changes (decreasing, increasing, and steady) in the height and length. Moreover, their changes are associated with the photospheric motions (converging, diverging, and shearing, respectively) of the underlying magnetic flux concentrations. This consistency indicates that the 3D structures are determined by the geometry of the magnetic flux concentrations. Figure 7 shows three scatter plots of heights of BPs and half-distances of magnetic flux separations for the three cases. The heights are systematically larger than the half-distances. In order to clarify the relationship between the heights and separation distances, we performed a simple statistical test using the autocorrelation method because they are time-series variations. The effective sample sizes determined by first-order autocorrelation coefficients were 10, 15, and 18 for the three cases and they are much lower than our sample sizes 108, 273, and 59. From the effective sample sizes, we estimated the expected correlation coefficients of a confidence level of 90% and they are 0.59, 0.46, and 0.41. The correlation coefficients of our samples are 0.85, 0.52, and 0.48 and they are higher than the 90% confidence level in this analysis. The high correlation coefficients with high confidence levels demonstrate that the height of EUV BPs highly depends on the separation distance of the underlying magnetic flux concentrations. A more direct comparison between the 3D structures and the photospheric motions is given in Figure 8. As mentioned in the previous sections, the changes in the length are consistent with the separation distance variations. More in-

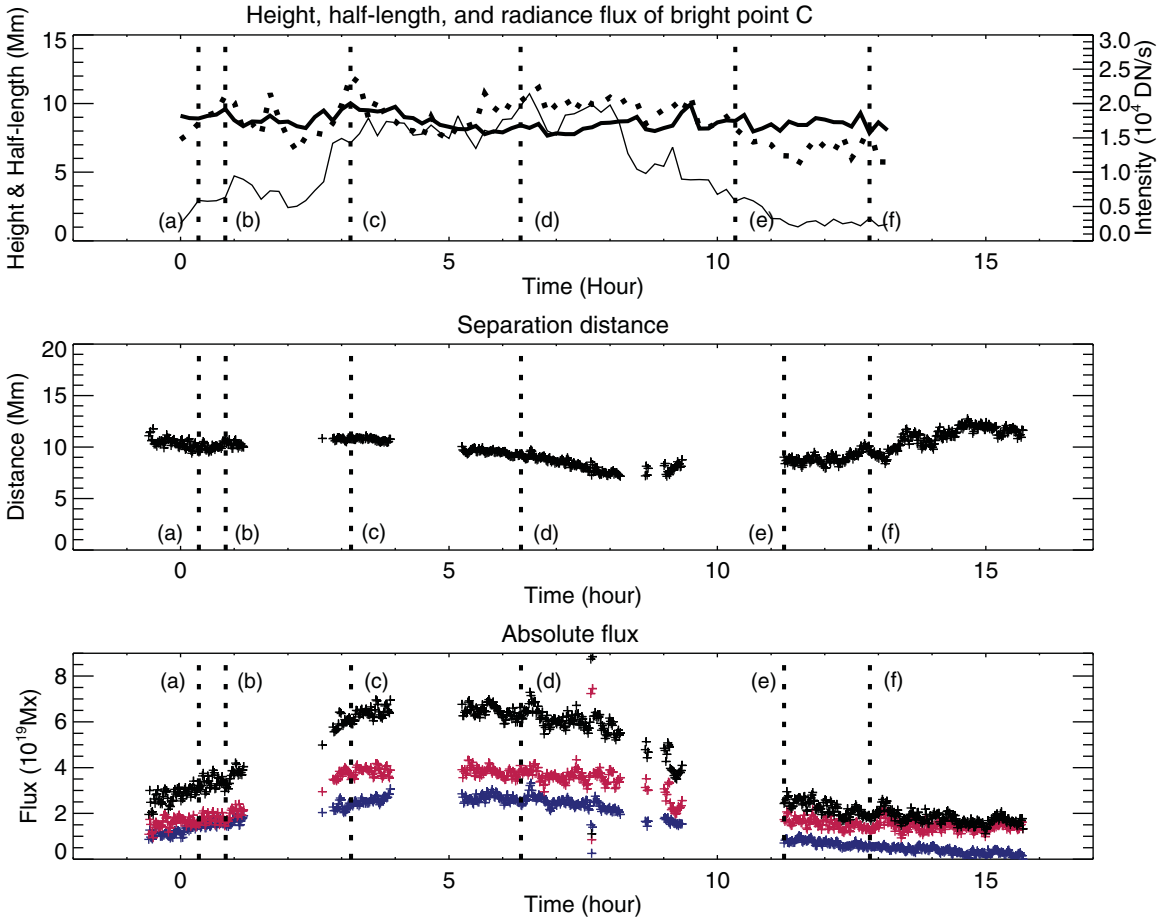

Figure 5. Temporal evolution of the physical parameters of case C. Other explanations are the same as Figure 1.
(A color version of this figure is available in the online journal.)

terestingly, it seems that the lengths are only barely within the outermost edges of the magnetic flux concentrations, suggesting that BPs should be a loop system connecting the two opposite magnetic poles (see, Longcope et al. 2001).

Second, there exists a couple of characteristics common to the three BPs, regardless of their distinct evolutions. (1) Each BP first appears as a faint loop system, its intensity reaches the maximum at the middle of its life, and then it disappears as a faint loop system. (2) The increase in magnetic flux is typically dominant in the initial phase and the decrease in the later phase. As a result, the intensity has a maximum near when the flux changes from increasing to decreasing and the intensity and the magnetic flux may be well correlated (Madjarska et al. 2003, and references therein).

Finally, we found no significant correlation between the magnetic fluxes and 3D structures. In case A, the height and length significantly decrease in the initial phase but the total magnetic flux increases simultaneously while the height/length and the total magnetic flux increase together in the initial phase of case B. Furthermore, the total magnetic flux of case C significantly increases in the first half and then decreases in the second half but there is no significant change in the 3D structure during its life. In a similar way, there exists no significant correlation between the 3D structure and intensity. This finding indicates that the 3D structure is mainly determined by the geometry of two opposite magnetic flux concentrations rather than the amount of magnetic fluxes.

Our findings suggest that magnetic reconnection should occur under all kinds of photospheric motions including converging motions. Priest et al. (1994) proposed a converging flux model: two opposite magnetic flux concentrations initially unconnected approach each other and magnetic reconnection can occur at an X-type null point. As a consequence of magnetic reconnection, the two opposite magnetic flux concentrations are connected by magnetic field lines below the X-type null point and the plasmas near the reconnected magnetic field lines are heated to have X-ray and/or EUV emissions. According to this scenario, the maximum height of the emission should be equal to half of the separation distance of two converging magnetic flux concentrations, so that the height may decrease during the life, as seen in case A (Figure 1). However, case B shows diverging motions within 13 hr associated with the increasing height and length, indicating that the converging motion may not be a necessary and sufficient condition for magnetic reconnection. Nevertheless, we cannot discard the converging motions as a driving source of magnetic reconnection, taking into account the sizes of two opposite magnetic fluxes. In case the amount of magnetic flux of one or both the opposite concentrations increases due to flux emergence or coalescence with unresolved flux elements (Lamb et al. 2008) and then the size increases during the diverging phase, it may be an alternative effect of the converging motion. For instance, there is no significant increase in the minimum distance of case B in the diverging phase ($t \leqslant 13$ hr) as shown in Figure 8 (middle panel) and there is significant increase in positive flux during the phase as shown in Figure 3 (bottom panel), implying that the two poles are associated with diverging photospheric motions but they are converging owing to the flux growth. It has been widely accepted

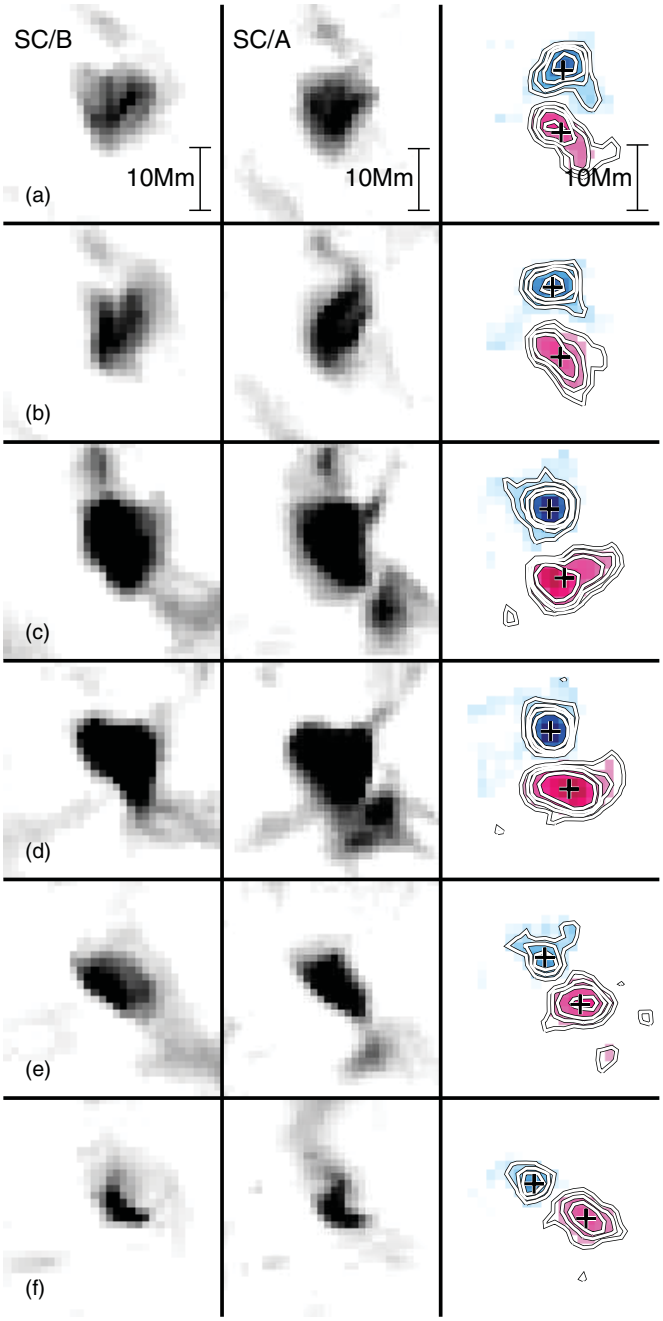

Figure 6. Morphological variation of case C at the times (a)–(f) in Figure 5. Other explanations are the same as Figure 2.

(A color version of this figure is available in the online journal.)

that flares are associated with magnetic flux emergences (e.g., Wang et al. 2004) and the nature of BPs may not be so different from the normal flares' (Shimojo & Shibata 1999).

The separator reconnection model proposed by Longcope (1998) can explain the magnetic reconnection under the shearing of two opposite magnetic flux concentrations, including the converging and diverging motions. Magnetic reconnection occurs on the separator field lines owing to the interaction between two initially unconnected opposite magnetic flux concentrations and horizontal background magnetic fields and could heat up the plasmas along this separator field lines. As a result, the 3D structure of subsequent X-ray/EUV BPs is predicted to depend on the geometry of the separator. Since this geometry is different from the one of magnetic field lines connecting a bipole, the length of a BP could be longer than the separation distance. Longcope et al. (2001) showed that a portion of 37% of BPs which were investigated are longer than the distance between the centers of the underlying magnetic flux concentrations. It is significant to note that our results seen in Figure 8 show that the lengths of BPs do not exceed the distances between the outermost edges of the bipoles, which may indicate that the BPs are the magnetic flux loops connecting bipoles. Nevertheless, we cannot fully rule out this model. In case the heated plasma along the separator field lines quickly moves along the reconnected magnetic field lines, the plasma can be observed as a loop system connecting the two underlying magnetic flux concentrations, even if the geometry of the separator field lines differ much from the one of the magnetic field lines. This is what we see in the normal flaring loop observations (e.g., Masuda et al. 1994) and models (e.g., Tsuneta 1997).

Our results show clearly that the magnetic fluxes do not affect the 3D structures. On the other hand, the amount of fluxes seems to be related to the variations of intensity of BPs (Madjarska et al. 2003). This fact can be interpreted that the variations of magnetic fluxes may be a proxy of the amount of released energy through magnetic reconnection. It is significant to note because it may tell us the role of small-scale magnetic fluxes in the large-scale coronal heating (Schrijver et al. 1998; Galsgaard et al. 2000; Close et al. 2004, 2005; von Rekwski et al. 2006). However, we provided only three cases so that it is hard to generalize to all the BPs. Accordingly, we postpone the discussion and conclusion regarding the role of the amount of the underlying magnetic fluxes in BPs.

In addition, we also investigated the multi-thermal nature of EUV BPs (Simon & Noyes 1972; Simon et al. 1974; Habbal & Withbroe 1981; van Driel-Gesztelyi et al. 1996; Kwon et al. 2010) using four passband images. Kwon et al. (2010) analyzed 210 EUV BPs selected from 11 snapshot images separated by about a month and found that the lengths are about twice the heights and the height and morphology depend on the passbands (temperature), indicating that a BP is a semi-circular and multi-temperature loop system. Note that they did not consider their evolutionary phases. Hence, it may be difficult to conclude that their findings are general characteristics over the whole lives of BPs. Figure 9 shows the height differences among four passbands whose peak temperatures of the filter response functions are about $10^{6.0}$ (171 Å), $10^{6.2}$ (195 Å), $10^{6.4}$ (284 Å), and $10^{4.9}$ K (304 Å; Wülser et al. 2004). The average heights over the entire lives at 171, 195, 284, and 304 Å are 6.7, 8.9, 7.1, and 5.9 Mm, respectively. As seen in this figure, the heights of the BPs at 195 Å are systematically higher than those at the other passbands and the BPs at 304 Å are located at the lowest parts of these structures. In the case of the BPs at 284 Å versus 195 Å, the heights of BPs at 195 Å are slightly higher than the ones at 284 Å even though the peak temperature of 284 Å is higher than the one of 195 Å. This result suggests more complicated loop system of which the hottest part (284 Å) is located between the cooler parts (171 Å and 195 Å). Kwon et al. (2010) compared the filter response functions and electron densities in BPs and conclude that 284 Å images are contaminated with cool plasmas and the hotter plasma may be located at the higher part of a loop system.

The correlation coefficients may provide us with a clue to figure out the 3D and multi-thermal structure of BPs. In the comparison of the heights among the four passbands, all the correlation coefficients are above the 99% confidence level.

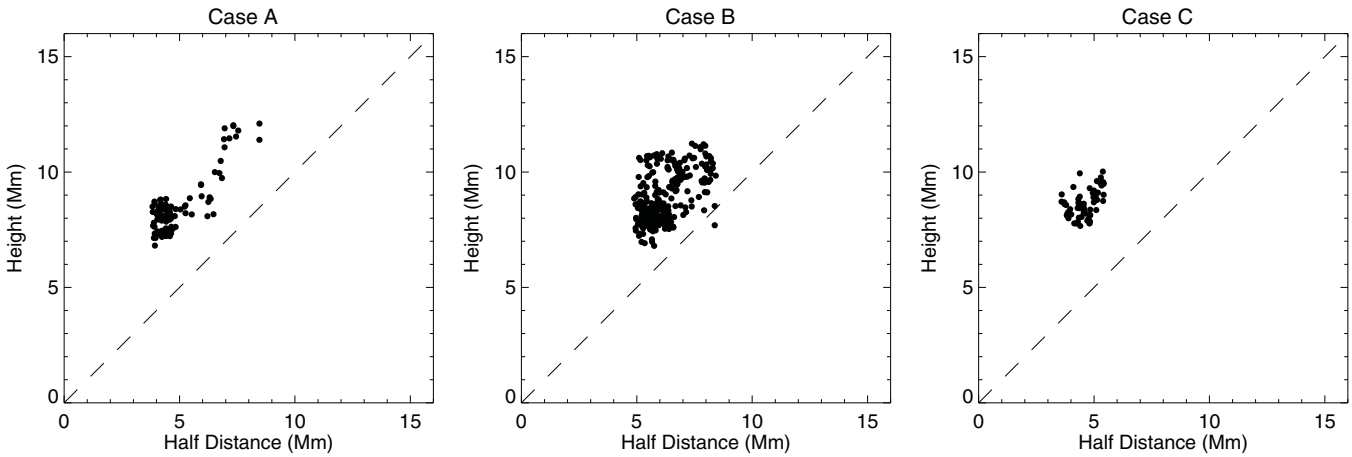

Figure 7. Scatter plots of height vs. half-distance of underlying magnetic flux concentrations. The distances are measured from the center of a signed magnetic pole to the center of the opposite pole.

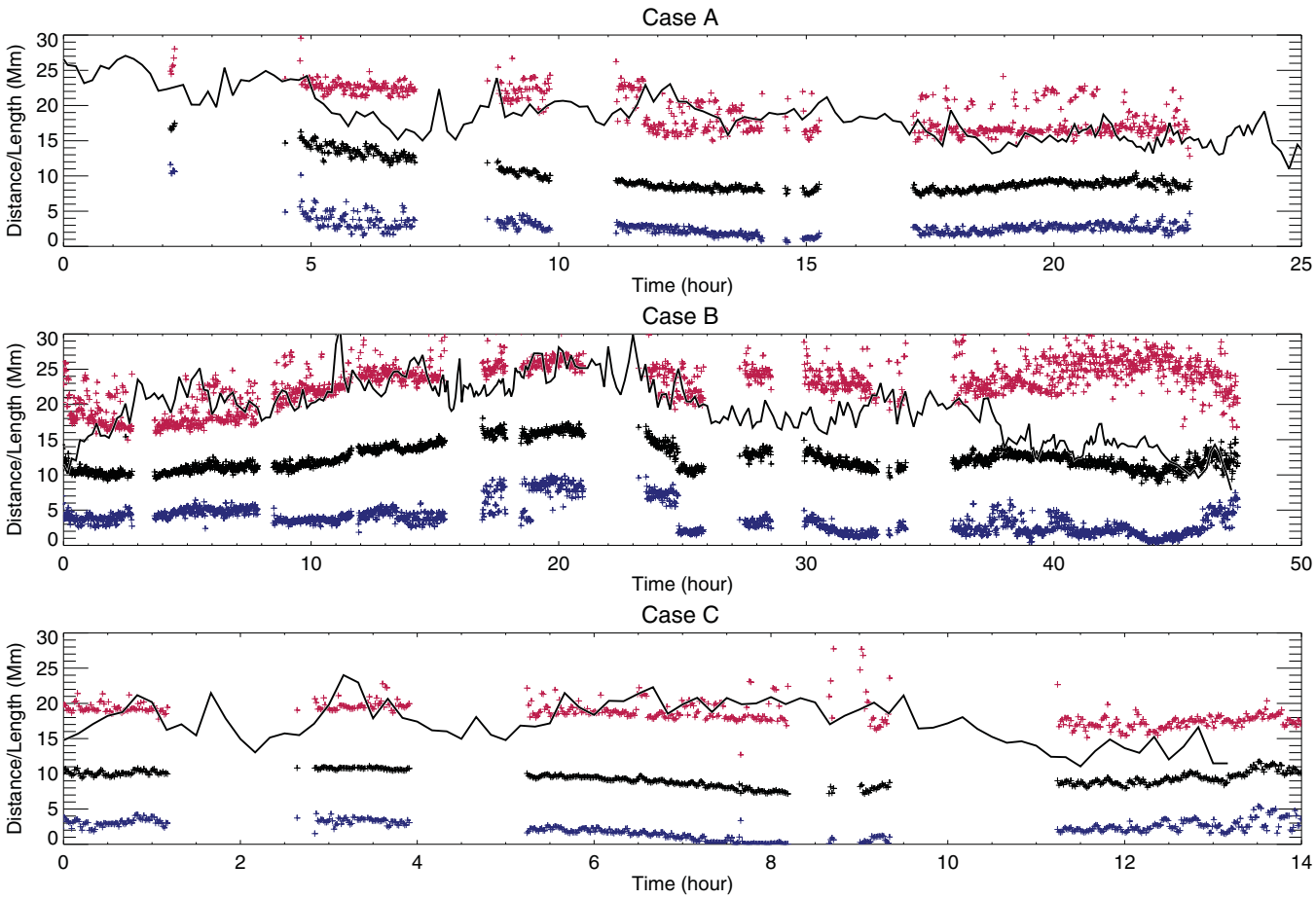

Figure 8. Time variations of lengths of BPs and distance of two opposite magnetic flux concentrations. The red, blue, and black crosses refer to the maximum, minimum, and center distances considering the sizes of the corresponding magnetic flux concentrations, respectively. The solid curves correspond to the lengths of the BPs.

(A color version of this figure is available in the online journal.)

The correlation coefficients are 0.44, 0.29, 0.21, and 0.68 between the heights, 195 Å versus 171 Å, 195 Å versus 304 Å, 171 Å versus 304 Å, and 284 Å versus 195 Å, respectively. The high correlation coefficients among BPs at 171, 195, and 284 Å may indicate that they belong to the same loop system. On the other hand, BPs at 304 Å have relative low correlation coefficients with the other three passbands but they are above the 99% confidence level. For this reason, the BPs at 304 Å can be interpreted as cool legs of the loop system. This is consistent with the previous results of Kwon et al. (2010).

Figure 10 shows scatter plots of heights and half-lengths. The correlation coefficients are 0.79, 0.47, and 0.18, respectively. In this case, the effective sample sizes are 20, 29, and 34 and the expected correlation coefficients of the 95% confidence level are

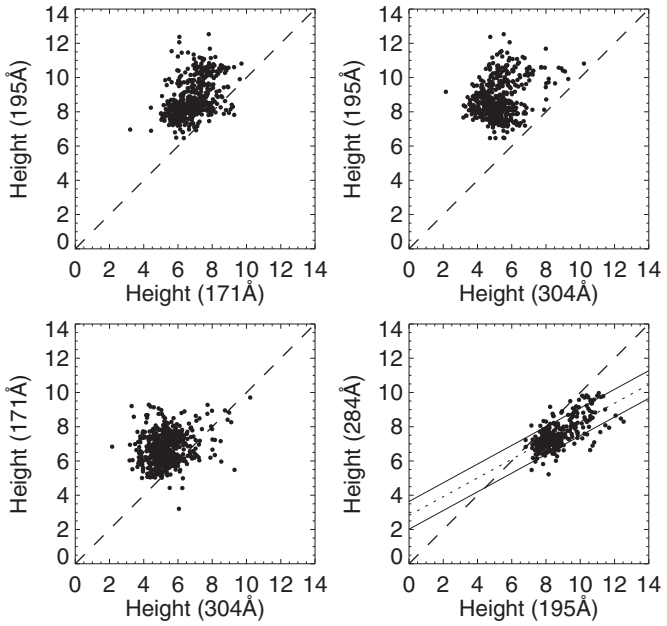

Figure 9. Scatter plots of heights at 195 Å vs. 171 Å (top left), 195 Å vs. 304 Å (top right), 171 Å vs. 304 Å (bottom left), and 284 Å vs. 195 Å (bottom left) for all the cases in each panel. Dotted line denotes the result of linear regression and two solid lines show the standard deviation of the heights at 284 Å subtracted by the linear component.

0.47, 0.38, and 0.35. The correlation coefficient for case A is the highest (above the 99% confidence level) because this BP shows a single loop system during its life except at time (b) and (c) in Figure 2. The reason why case C has the lowest coefficient may be due to the smallest standard deviation (0.5 Mm) of heights since case C shows no significant change in its height. In general, as seen in Figure 10, the lengths are more scattered than heights. The lengths are measured in images above the background and noise level so that these results may be sensitive to the background and noise subtractions while the heights are measured from the intensity weighted center so that the results may not so sensitive to the subtractions. This may be the reason why case C does not show a high correlation coefficient between the height and length. Despite the small correlation coefficient of case C, this figure demonstrates that the heights and half-lengths are nearly identical in all the cases. Together with the above discussion, these results demonstrate that the multi-temperature and semi-circular loop system is more or less a general character of BPs.

5. SUMMARY AND CONCLUSION

We have presented 3D structures and evolutions of EUV BPs, observed by SECCHI/ EUVI on board *STEREO* spacecraft. We measured heights and lengths of EUV BPs, as the components of the 3D structures and found out the presence of three distinct changes in them (decreasing, increasing, and steady). These changes are associated with the converging, diverging, and shearing motions of the underlying magnetic flux concentrations, respectively. It is significant that the height and the length are well correlated with the separation distance of two opposite magnetic flux concentrations and the length seems to be less than or equal to the distance between the outermost edges of the two opposite magnetic flux concentrations. These facts demonstrate that the 3D structures are mostly determined by the geometry of the underlying magnetic flux concentrations and BPs are a loop system. The geometry of the loop system may represent the reconnected magnetic field lines rather than the separator field lines. Irrespective of the distinct changes, common evolutionary features are found in the intensities and the magnetic fluxes. In addition, they all have multi-temperature structures whose hot loops are overlying cooler loops with a remarkable correlation between the height and length. We could not find out direct relationship between the 3D structures and the amount of magnetic fluxes. We compared the characteristics of the three BPs with two models, the converging flux model and the separator reconnection model, and we found that some our findings are consistent with these models. However, the varying size and internal structure of the underlying magnetic flux concentrations which are neglected in these models seem to be significant for the formation and the evolution of BPs. In conclusion, BPs may be regarded as a multi-thermal and semi-circular loop system formed by magnetic reconnection, like the normal flaring loops.

This work generalizes some characteristics of 3D structures of BPs, such as multi-temperature and semi-circular loop system by looking into the detailed evolutionary histories of the three distinct cases. On the other hand, it needs to be extended to a larger population BPs to generalize the new characteristics found by this work, such as the three distinct types of evolution and their relationship with the underlying magnetic fluxes. In addition, we postpone the discussion of the role of the amount of magnetic fluxes in the evolutions of EUV BPs. The higher spatial and temporal resolutions of data taken from the *Solar Dynamic Observatory* will provide us with a greater statistical analysis of the three distinct types of evolution, seeking the changes of

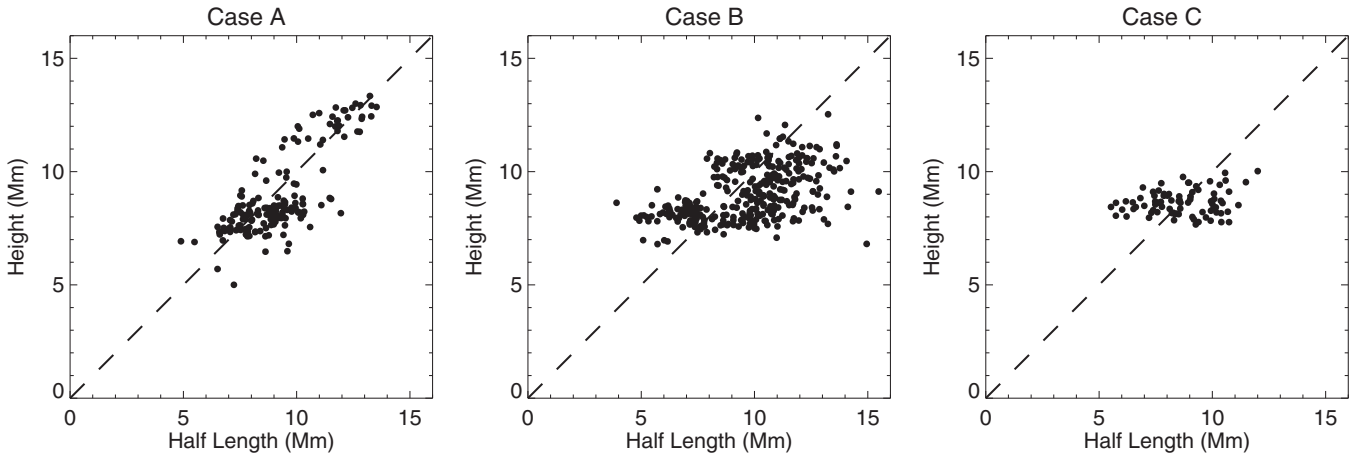

Figure 10. Scatter plots of height vs. half-length for cases A–C, respectively.

lengths of BPs as a proxy of the 3D structure and the changes of properties of the underlying magnetic flux concentrations.

We are grateful to the referee for a number of constructive comments. This work was supported by NASA grant NNX10AN10G and the Korea Research Foundation Grant funded by the Korean Government (KRF-2008-220-C00022).

REFERENCES

Chae, J., Moon, Y.-J., & Pevtsov, A. A. 2004, ApJ, 602, L65
Chae, J., Moon, Y.-J., Wang, H., & Yun, H. S. 2002, Sol. Phys., 207, 73
Close, R. M., Parnell, C. E., Longcope, D. W., & Priest, E. R. 2004, ApJ, 612, 81
Close, R. M., Parnell, C. E., Longcope, D. W., & Priest, E. R. 2005, Sol. Phys., 231, 45
Galsgaard, K., Parnell, C. E., & Blaizot, J. 2000, A&A, 362, 395
Golub, L., Krieger, A. S., Harvey, J. W., & Vaiana, G. S. 1977, Sol. Phys., 53, 111
Golub, L., Krieger, A. S., Silk, J. K., Timothy, A. F., & Vaiana, G. S. 1974, ApJ, 189, L93
Golub, L., Krieger, A. S., & Vaiana, G. S. 1975, Sol. Phys., 42, 131
Golub, L., Krieger, A. S., & Vaiana, G. S. 1976, Sol. Phys., 50, 311
Habbal, S. R., & Withbroe, G. L. 1981, Sol. Phys., 69, 77
Harvey, K. L., & Martin, S. F. 1973, Sol. Phys., 32, 389
Howard, R. A., Moses, J. D., Vourlidas, A., et al. 2008, Space Sci. Rev., 136, 67
Krieger, A. S., Vaiana, G. S., & van Speybroeck, L. P. 1971, in IAU Symp. 43, Solar Magnetic Fields, ed. R. Howard (Dordrecht: Reidel), 397
Kwon, R.-Y., Chae, J., & Zhang, J. 2010, ApJ, 714, 130
Lamb, D. A., DeForest, C. E., Hagenaar, H. J., Parnell, C. E., & Welsch, B. T. 2008, ApJ, 674, 520
Longcope, D. W. 1998, ApJ, 507, 433
Longcope, D. W., Kankelborg, C. C., Lelson, J. L., & Pevtsov, A. A. 2001, ApJ, 553, 429
Madjarska, M. S., Doyle, J. G., Teriaca, L., & Banerjee, D. 2003, A&A, 398, 775
Martin, S. F., & Harvey, K. H. 1979, Sol. Phys., 64, 93
Masuda, S., Kosugi, T., Hara, H., Tsuneta, S., & Ogawara, Y. 1994, Nature, 371, 495
Priest, E. R., Parnell, C. E., & Martin, S. F. 1994, ApJ, 427, 459
Schrijver, C. J., Title, A. M., Harvey, K. L., et al. 1998, Nature, 394, 152
Shimojo, M., & Shibata, K. 1999, ApJ, 516, 934
Simon, G. W., & Noyes, R. W. 1972, Sol. Phys., 22, 450
Simon, G. W., Seagraves, P. H., Tousey, R., Purcell, J. D., & Noyes, R. W. 1974, Sol. Phys., 39, 121
Tsuneta, S. 1997, ApJ, 483, 507
van Driel-Gesztelyi, L., Schmieder, B., Cauzzi, G., et al. 1996, Sol. Phys., 163, 145
von Rekowski, B., Parnell, C. E., & Priest, E. R. 2006, MNRAS, 366, 125
Wang, H., Qiu, J., Jing, J., et al. 2004, ApJ, 605, 931
Webb, D. F., Martin, S. F., Moses, D., & Harvey, J. W. 1993, Sol Phys., 144, 15
Wülser, J.-P., Lemen, J. R., Tarbell, T. D., et al. 2004, SPIE, 5171, 111
Zhang, J., Kundu, M. R., & White, S. M. 2001, Sol. Phys., 198, 347